



A proposal for the combined analysis of bone quantity and quality of human cortical bone by quasi-brittle fracture mechanics

Glynn Gallaway^a, Rachel K. Surowiec^b, Matthew R. Allen^{c,d}, Joseph M. Wallace^b, Laura J. Pyrak-Nolte^e, John A. Howarter^{f,g}, Thomas Siegmund^{a,*}

^a School of Mechanical Engineering, Purdue University, United States of America

^b Weldon School of Biomedical Engineering, Purdue University, United States of America

^c Department of Anatomy, Cell Biology, and Physiology, Indiana University School of Medicine, United States of America

^d Roudebush Veterans Administration Medical Center, United States of America

^e Department of Physics and Astronomy, Purdue University, United States of America

^f School of Materials Engineering, Purdue University, United States of America

^g Environmental and Ecological Engineering, Purdue University, United States of America

ARTICLE INFO

Keywords:

cortical bone
Fracture mechanics
Bone quality
Bone quantity
Fracture process zone

ABSTRACT

Quasi-brittle fracture mechanics is used to evaluate fracture of human cortical bone in aging. The approach is demonstrated using cortical bone bars extracted from one 92-year-old human male cadaver. In-situ fracture mechanics experiments in a 3D X-ray microscope are conducted. The evolution of the fracture process zone is documented. Fully developed fracture process zone lengths at peak load are found to span about three osteon diameters. Crack deflection and arrest at cement lines is a key process to build extrinsic toughness. Strength and toughness are found as size-dependent, not only for laboratory-scale experimental specimens but also for the whole femur. A scaling law for the length fracture process zone is used. Then, size-independent, tissue fracture properties are calculated. Linear elastic fracture mechanics applied to laboratory beam specimens underestimates the tissue toughness by 60%. Tissue fracture properties are used to predict the load capacity of the femur in bending within the range of documented data. The quasi-brittle fracture mechanics approach allows for the assessment of the combined effect of bone quantity and bone quality on fracture risk. However, further work is needed considering a larger range of subjects and in the model validation at the organ length scale.

1. Introduction

Fragility fractures at advanced age are linked to decreased quality of life and increased mortality risk (Teng et al., 2008). Osteoporosis treatments are among the least effective when compared to other common diseases (Leucht et al., 2015). Developing effective therapies to decrease fracture risk is critical to advancing health outcomes. Decisions on clinical intervention in bone diseases must be based on the best possible scientific methodology, Dapaah and Willett (2022). Osteoporosis assessment commonly relies on measurements of bone mineral density (BMD) through Dual-Energy X-ray Absorptiometry (DEXA), Aibar-Almazán et al. (2022). BMD is correlated to bone strength, but DEXA provides an imperfect assessment of fracture risk (Kanis et al., 2000; Lu et al., 2001). Consequently, other measures for bone health are needed (Schuit et al., 2004) and point to investigation of bone quality (Hernandez and Keaveny, 2006; Hernandez and van der Meulen, 2017).

Fracture mechanics (FM) theory underpins safety predictions for structures containing flaws subjected to mechanical loads. FM can inform on factors leading to fragility fractures beyond BMD/DEXA and strength (Granke et al., 2015; Dapaah et al., 2023) in pre-clinical and clinical conditions (Lloyd et al., 2017). FM properties of bone are documented to depend on age (Zioupos and Currey, 1998; Nalla et al., 2004a, 2006; Zimmermann et al., 2011), osteoporotic disease state (Giannoudis et al., 2007), and anatomical direction (Koester et al., 2008).

Linear elastic fracture mechanics (LEFM) provides fracture toughness as critical values of stress intensity factors (SIFs), Koester et al. (2008). However, such a single value property does not describe bone fracture because LEFM assumes the tissue as linear elastic and without significant damage before peak load. Such conditions are not commonly fulfilled in bone.

* Correspondence to: 585 Purdue Mall, West Lafayette, IN 47906, USA
E-mail address: siegmund@purdue.edu (T. Siegmund).

The J -integral quantifies non-linear contributions to fracture. Data of J vs. crack growth, Δa , establish the crack growth resistance (R) curve. For human cortical bone, R -curves depend on direction (Koester et al., 2008), age (Nalla et al., 2004a), and disease state (Lloyd et al., 2017). The steeply rising R -curve for transverse fracture of human cortical bone indicates a limited (intrinsic) resistance to crack initiation, but a strong (extrinsic) resistance to crack growth (Zimmermann et al., 2010; Launey et al., 2010). Extrinsic toughening mechanisms include microcracking, crack deflection at cement lines, and osteon pullout (Vashishth et al., 1997; Nalla et al., 2005; Barthelat, 2023). Fracture process zones (FPZs) were estimated to be hundreds of micrometers in length (Koester et al., 2008). Thus, conditions where the J -integral is a material property and characterizes the stress field near the crack tip are very rarely fulfilled in bone. To resolve this problem, a length scale needs to be included in the FM analysis.

Quasi-brittle fracture mechanics (QBFM) is specifically suited to analyze the fracture of materials with large FPZs to address the observed dependence of strength on structural size (Bažant, 1984; Bažant and Kazemi, 1990). QBFM seeks to determine inherent length scales and true, size-independent, fracture properties. Length scales are commonly obtained indirectly through multi-specimen approaches using either geometrically similar samples of multiple sizes (Bažant, 1984; Bažant and Kazemi, 1990; Ando et al., 1992; Wu et al., 2011; Tsouvalis and Anyfantis, 2012; Morgan et al., 2013; Kim et al., 2013; Moazzami et al., 2020), or identically-sized specimen with multiple crack lengths (Wu et al., 2011). Kim et al. (2013) used QBFM and a multi-specimen approach to characterize transverse fracture in a bovine femur and longitudinal fracture in the human humerus, Nalla et al. (2005). The FPZ length was obtained as ~ 5 mm for splitting fracture in the human humerus, Kim et al. (2013). This finding agrees with data on direct bridging measurements, Nalla et al. (2004b), and numerical simulations with cohesive zone models, Yang et al. (2006). For transverse fracture of bovine bone (Kim et al., 2013) obtain the FPZ length as 3.6 mm.

The critical distance approach introduces a length scale as the ratio between the LEFM fracture toughness and the critical stress, determined through multi-specimen experiments and model fits (Kasiri and Taylor, 2008). For bone, the approach was executed using notched specimen data, Kasiri and Taylor (2008) and indentation data (Ghoulil et al., 2022) for bovine and sheep bone indicating again the substantive extent of the length scale.

Challenges arise when applying length-scale dependent FM approaches to transverse fractures of long bones. Multi-specimen approaches are challenging to execute in the human bone due to limited material availability, location variability, and subject specificity. It is difficult to obtain a wide enough size range of samples for size-fitting due to limitations imposed by anatomical shape (Kim et al., 2013). A method to overcome the limits of multi-specimen approaches was proposed (Bažant and Li, 1996) but requires an additional plasticity solution.

We base our approach on direct measurements of FPZ length for transverse fracture in human cortical bone by use of in-situ FM experiments in the beamline of a 3D X-ray microscope. Similar in-situ methods for bone exist (Lowe et al., 2018; Peña Fernández et al., 2020; Karali et al., 2021), but FPZ lengths were not measured. Fracture processes in human cortical bone under transverse fracture were documented with image domains insufficient to capture the full FPZ (Koester et al., 2008). Surface measurements of crack growth (Nalla et al., 2005; Koester et al., 2008) inherently underestimate fracture progression. Here, we combine measurements of the FPZ length with the size effect extrapolation technique derived from general principles of QBFM, Fakhimi and Tarokh (2013), Galouei and Fakhimi (2015) and Tarokh et al. (2017), to obtain true fracture properties and inherent length scales from single specimen size measurements.

A case study on applying QBFM to bone fracture analysis is undertaken. Tissue fracture properties are determined and related to bone microstructure and whole bone femoral shaft bending failure loads are

analyzed. QBFM analysis is used for the investigation of the coupled effects of bone quantity (cortical thickness) and bone quality (tissue fracture properties). This is in contrast to the common approach where bone nominal strength is a material property, and quantity and bone quality are considered independently. Implications of aging, disease, and therapies are discussed.

2. Methods

2.1. Theory

LEFM applies damage at the crack tip is confined to a domain very small relative to the specimen size. For peak force, P_u , on a SEN(B) sample (height, b , depth, d , initial notch, a_0 , span, s) subjected to 3-point-bending (TPB), the LEFM fracture toughness is

$$G_{LEFM} = \frac{P_u^2}{E' b^2 d} g_{(\gamma)}(\alpha_0) \quad (1)$$

with E' the plane strain elastic modulus, $\alpha_0 = a_0/d$ the normalized initial crack length, and g_{γ} a configuration function. Configuration functions are commonly provided for SIFs, $K = \sqrt{G/E'}$ and $g = k^2$. Solutions for k follow from Guinea et al. (1998), Appendix A.

QBFM incorporates the FPZ length, L , and introduces a size effect into the analysis. The effective normalized crack length α_{eff} is:

$$\alpha_{eff} = \frac{1}{d} \left(a_0 + \frac{L}{2} \right) \quad (2)$$

A linear decay of crack bridging tractions relative to the crack tip introduces the factor of $1/2$. The QBFM fracture toughness is

$$G_{QBFM} = \frac{P_u^2}{E' b^2 d} g(\alpha_{eff}) \quad (3)$$

where $L = L_c$ at P_u .

G_{LEFM} , L_c , and G_{QBFM} depend on specimen size (Bažant and Kazemi, 1990). Thus, true, size-independent, measures describing material failure are needed. Tissue FPZ length, L_{∞} , tissue strength, S_{∞} , and tissue fracture toughness, G_{∞} , are obtained in the limit $d \rightarrow \infty$. Such a condition is experimentally not viable in bone.

Any specimen (or structure) is characterized by the brittleness number, β , Bažant and Kazemi (1990):

$$\beta = \frac{2d}{L_{\infty}} \frac{g(\alpha_0)}{g'(\alpha_0)} \quad (4)$$

The value of β characterizes conditions of LEFM ($\beta > 10$), QBFM ($0.1 < \beta < 10$), or a strength dominated regime ($\beta < 0.1$) (Bažant and Kazemi, 1990). Following Fakhimi and Tarokh (2013), Galouei and Fakhimi (2015) and Tarokh et al. (2017), L_c scales with β as:

$$L_c = \frac{L_{\infty} \beta}{1 + \beta} \quad (5)$$

Consequently, L_{∞} is:

$$L_{\infty} = L_c \left[1 - \frac{L_c}{2d} \frac{g'(\alpha_0)}{g(\alpha_0)} \right]^{-1} \quad (6)$$

Tissue fracture toughness G_{∞} follows from β and G_{LEFM} , Bažant and Kazemi (1990):

$$G_{\infty} = G_{LEFM} \frac{1 + \beta}{\beta} \quad (7)$$

Furthermore, the tissue strength S_{∞} is

$$S_{\infty} = c_n \sqrt{\frac{2G_{\infty} E'}{L_{\infty} g'(\alpha_0)}} \quad (8)$$

The size-dependent, nominal strength, σ_N is, Bažant and Kazemi (1990):

$$\sigma_N = \frac{S_{\infty}}{\sqrt{1 + \beta}} \quad (9)$$

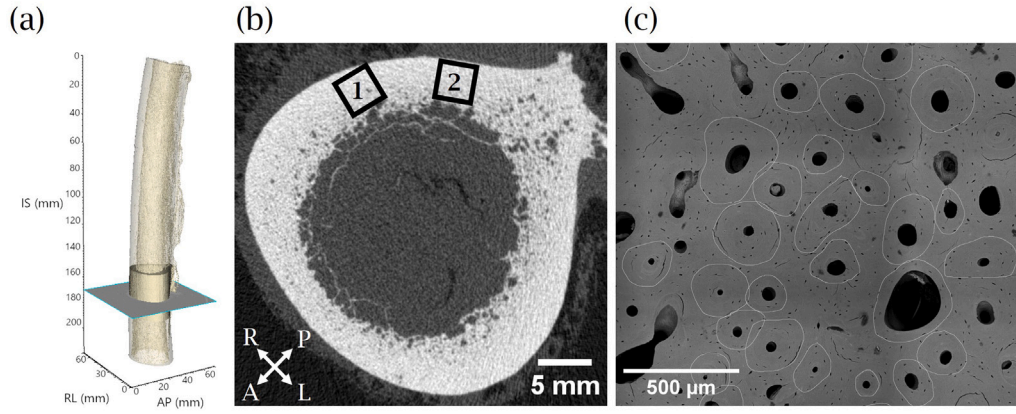


Fig. 1. (a) HR-pQCT image of the femoral shaft (translucent), section extracted indicated (opaque). (b) Image slice of (a) with specimen locations. (c) Backscatter SEM image of bone cross-section with cement lines outlined used to determine On.Dm., Beam 1. P = Posterior, A = Anterior, R = Right, L = Left.

The osteon diameter, On.Dm, is the characteristic microstructure length scale in cortical bone. The tissue FPZ length L_∞ then relates to On.Dm via the microstructure efficiency factor η :

$$L_\infty = \eta \cdot \text{On.Dm} \quad (10)$$

The critical load P^* for femoral shaft bending fracture can be predicted. The analysis assumes the femur as a thick-walled pipe under bending (Ritchie et al., 2008; Carriero et al., 2014; Bartlow et al., 2018), Appendix B. Bone geometry is given by cortical wall thickness, Ct.Th, mean cortical diameter, Ct.Dia, and the resulting cortical area, Ct.Ar. The whole bone diaphysis possesses length FDL. Assuming naturally occurring defects with size \sim On.Dm, the configuration function for the whole bone under TPB conditions, \tilde{g} and its derivative \tilde{g}' , are:

$$\tilde{g}(\vartheta) = \tilde{k}^2(\vartheta) \quad (11)$$

$$\tilde{g}'(\vartheta) = \frac{d}{d\vartheta} \tilde{g}(\vartheta) \quad (12)$$

with ϑ the center angle for a secant to the femur cross-section at depth On.Dm. Then, the brittleness number β^* for the long bone is:

$$\beta^* = \frac{\text{Ct.Dia} + \text{Ct.Th}}{\eta \text{On.Dm}} \frac{\tilde{g}(\vartheta)}{\tilde{g}'(\vartheta)} \quad (13)$$

Finally, the critical load for femoral shaft bending fracture, P^* , is:

$$P^* = \frac{\text{Ct.Ar}}{\tilde{c}_N} \frac{S_\infty}{\sqrt{1 + \beta^*}} \quad (14)$$

with \tilde{c}_N a convenience factor, Appendix B.

2.2. Materials

We demonstrate the principle of the approach in a case study ($n = 2$). The diaphysis of a human (92-year-old, male, femur diaphysis length FDL = 21.9 cm) cadaveric femur was obtained through the Indiana University School of Medicine Anatomical Donation Program. A section was extracted at the mid-diaphysis and imaged with HR-pQCT (Gallaway et al., 2024a), Fig. 1A, with average cortical thickness Ct.Th = 6.9 mm and mean cortical diameter Ct.Dia = 31.3 mm, Fig. 1B. Considering cortical wall curvature and internal porosities, the largest prismatic bars extractable from the section were of nominal size 4.0 mm \times 4.0 mm \times 28.0 mm. Bars were cut using a low-speed saw with a cBN blade (Buehler, Illinois, USA) and ground to square. A notch, $a_0/d \approx 0.5$, was cut into the endosteal face using a 200 μ m diamond blade on the same saw. Specimens were kept hydrated with phosphate-buffered saline (PBS). The bone-volume-to-total-volume ratio (BV/TV) in the volume above the notch was determined from un-damaged states by 3D X-ray microscopy (Section 2.3) by thresholding the image for dense tissue (Simpleware ScanIP, Synopsys, California, USA). The longitudinal plane strain elastic modulus of the dense tissue was assumed

Table 1

Measures of beam geometry and bone tissue microstructure.

	b [mm]	d [mm]	a_0 [mm]	BV/TV [%]	E' [MPa]	On.Dm [μ m]
Beam 1	4.0	4.0	1.8	92.5	17,649	242 (SD: 62)
Beam 2	4.0	3.8	1.7	90.0	17,170	284 (SD: 51)

to be $E'_0 = 19.08$ GPa, Mirzaali et al. (2016). The modulus of the beams was determined as $E' = E'_0(\text{BV/TV})$. The osteon diameter, On.Dm, was measured on polished sections (Fig. 1C) using backscatter SEM images (Britz et al., 2009). Using ImageJ, a grid is imposed on the images and On.Dm is determined as the Feret Diameter for at least 40 On.Dm measures. Table 1 summarizes beam and tissue measures.

Samples are controls from a larger study on the effects of pharmaceutical treatment on bone. Specimens were incubated for 14 days at 37 $^\circ$ C in PBS supplemented with 1% penicillin-streptomycin and 0.04% vol/vol dimethyl sulfoxide, Gallant et al. (2014) with solution change every 2 days. After, the samples were kept frozen at -20 $^\circ$ C, and defrosted at 4 $^\circ$ C overnight before experiments.

2.3. Experiments

In-situ fracture experiments were conducted in a TPB frame with span $s = 20$ mm (Deben CT5000N Deben, Bury St. Edmunds, UK) in 3D X-ray microscope (XRADIA 510 Versa, Carl Zeiss AG, Baden-Württemberg, Germany) (Fig. 2).

Experiments were conducted in air at ambient temperature and humidity. Specimens are wrapped in a plastic film slit at the notch to reduce surface dehydration. Displacement U was applied at $\dot{U} = 0.1$ mm/min except during imaging ($\dot{U} = 0$). Load cell outputs were monitored and recorded. The first 3D image was obtained at the onset of non-linearity. Subsequently, U was increased to raise the load by 10 N and another image was obtained. This sequence was repeated 6 times. 3D X-ray images were acquired at resolution 4.5 μ m, exposure time 5 s, 801 projections, 120 kV, 10 W, 4 \times objective, and a LE2 filter. Individual image acquisitions required 90 min. The estimated overall radiation dosage was 54 Gy and is expected to not influence the fracture properties of bone (Schmidt et al., 2022). X-ray projections were processed through XRADIA Scout-and-Scan Reconstructor and analyzed using Simpleware, Appendix C. Crack mouth opening was measured on each image stack using 3D measurement tools in Simpleware at 3 points along the crack mouth in the first image slice containing the full crack mouth. Crack mouth opening displacement, $CMOD$, was calculated with respect to the initial crack mouth opening before loading.

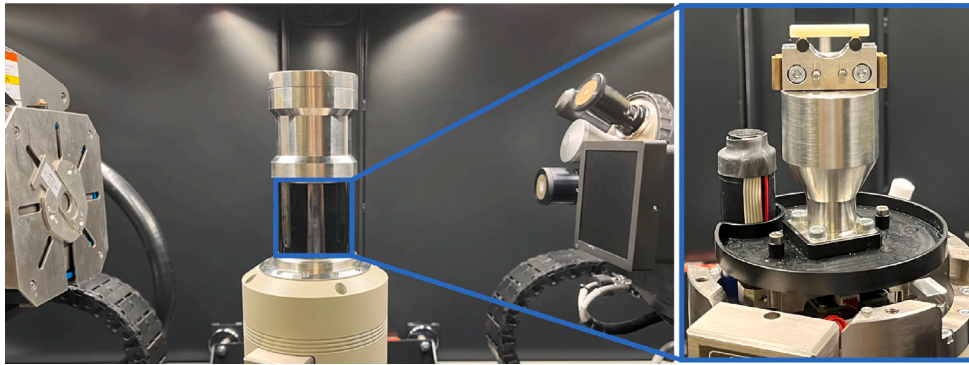


Fig. 2. Experimental setup for in-situ fracture mechanics experiments in 3D-X-ray microscope with X-ray source (left), load rig (center), X-ray detector (right). Detail view of inside of load rig (top jaw removed): specimen and base of TPB fixture.

Table 2
Specimen specific fracture data (L_c , β , G_{LEFM} , G_{QBFM}) and tissue fracture properties (L_∞ , η , G_∞ , S_∞).

	L_c [μm]	L_∞ [μm]	β [-]	η [-]	G_{LEFM} [N/mm]	G_{QBFM} [N/mm]	G_∞ [N/mm]	S_∞ [MPa]
Beam 1	486.1	776.0	1.68	3.2	0.658	0.906	1.050	104.3
Beam 2	559.3	890.0	1.69	3.1	0.500	0.769	0.797	83.6
Average	522.7	833.0	1.69	3.2	0.579	0.838	0.924	94.0

3. Results

The growth of the FPZ during loading is depicted in Fig. 3, (Galloway et al., 2024a). Material separation is first observed in small volumes at the notch tip, away from the free surfaces, Fig. 3(a,f). Subsequently, the FPZ grows in length and spreads laterally. The FPZ intersects with the free surface at loading stages far beyond the first defect initiation, Fig. 3(d,i). In the image taken past the peak load, Fig. 3(e,j), the FPZ is separated from the initial notch, and the FPZ is fully developed. The FPZ is tortuous and interacts with the microstructure. Movies for Fig. 3 are provided as supplemental material.

Force F - $CMOD$ data, and L - $CMOD$ data are shown in Fig. 4, (Galloway et al., 2024b). FPZ length increases throughout loading and saturates to L_c at the maximum load P_u . Force data depicted are those at the start of each image hold step as a limited amount of load relaxation occurs during each load step, Appendix D.

The relevance of the FPZ becomes evident when considering the crack growth resistance (R) curve. R -curves are given as G_{QBFM} vs. L , Fig. 5. Crack initiation toughness is low and followed by a substantial rise in the R -curve. Table 2 summarizes specimen specific values (L_c , β , G_{LEFM} , G_{QBFM}) together with the calculated tissue fracture properties (L_∞ , η , S_∞ , G_∞). The present fracture experiments are in the quasi-brittle regime ($\beta < 10$). Thus, the specimen-specific measures are only apparent properties and deviate from the true tissue properties to a significant extent.

Details of the saturated FPZ are shown in Fig. 6 (Beam 1). Cement lines play a key role in the transverse fracture of human cortical bone by inducing crack deflection and debonding of the osteons, while the osteon itself bridges the crack. Tissue FPZ length L_∞ is thus indeed related to On.Dm. Tissue about three osteons in front of the fully separated crack tip is responsible for crack bridging, Table 2.

The QBFM analysis is applied to the femur diaphysis under TPB conditions using data from Tables 1 and 2. The brittleness numbers for the femur diaphysis ($\beta_1^* = 5.01$, $\beta_2^* = 4.69$) remain in the quasi-brittle regime of $0.1 < \beta^* < 10$. Predicted values for P^* are 2.778 kN (Beam 1 data) and 2.289 kN (Beam 2 data). These values of P^* align with measured failure data for femoral shafts under quasi-static loading in Mather (1967) where bending failure loads of mean 2.9 kN and standard deviation of 0.7 kN are given.

The model, Eq. (14), can be used to compute individual and combined effects of bone quantity and measures on whole bone strength. Changes to P^* from $\pm 20\%$ changes to cortical thickness Ct.Th (a bone quantity measure), tissue strength S_∞ (an intrinsic quality measure), and η (an extrinsic quality measure) are considered. Results are for average data of Table 2. Alternate results based on Beam 1 or Beam 2 data affect the predictions by less than 0.04%, Supplementary Data. Bone quality and quantity factors are inherently coupled in the biological system but understanding the individual effects is useful. Fig. 7 describes how each factor individually relates to the critical load P^* . Parameters Ct.Th, S_∞ and η are linearly related to P^* while P^* is nonlinearly dependent on η . The critical load P^* is most strongly affected by S_∞ , followed by Ct.Th and η . The model predicts nonlinear interaction between the bone quality parameters S_∞ and η , Fig. 8. A loss in S_∞ and η leads to a loss in P^* more significant than expected from a linear interaction. The model also predicts the gradient of $P^*(S_\infty, \eta)$ to decrease with a loss in Ct.Th. A loss in Ct.Th also causes a decrease in β^* such that the strength limit of the quasi-brittle fracture response is approached. This finding indicates the need for smaller changes in bone quality to maintain structural integrity as long as Ct.Th is maintained.

4. Discussion

Cortical bone from the femur of a 92-year-old male emerges as a quasi-brittle solid with a pronounced FPZ. This is the first study to report high-resolution 3D imaging of fully developed FPZs, Fig. 3, for human cortical bone in transverse fracture using specimens of size corresponding to the cortical wall thickness. The two specimens considered vary in On.Dm, but in both specimens the fully developed FPZ is $L_c \approx 3 \times \text{On.Dm}$. While the specimens possess rather similar LEFM toughness, the differences in On.Dm are reflected in the QBFM toughness and the intrinsic tissue fracture properties. While FPZ length varies across the specimens extracted, the present results point to more general insights into bone fracture enabled by QBFM. The FPZ introduces a size dependence of the fracture characteristics. At the present loading rate, cement line debonding, osteon crack bridging, and interstitial matrix fracture emerge as the key mechanisms of crack growth, Fig. 6, in agreement with Yeni et al. (1997), Idkaidek and Jasiuk (2017), Gustafsson et al. (2019) and Demirtas et al. (2023). We find that QBFM conditions prevail in both the laboratory specimens and in the corresponding whole bone. Therefore, QBFM analysis is indispensable for establishing tissue fracture properties. Then, QBFM provides a pathway to connect laboratory measurements of fracture properties to predictions of whole-bone fracture risk. Such arguments apply to studies using lab scale specimens extracted from cadaveric donor bone to assess bone fracture characteristics (Nalla et al., 2004a; Koester et al., 2008; Granke et al., 2015; Dapaah et al., 2022) or to the use of bone biopsies to assess patient fracture risk (Lloyd et al., 2017).

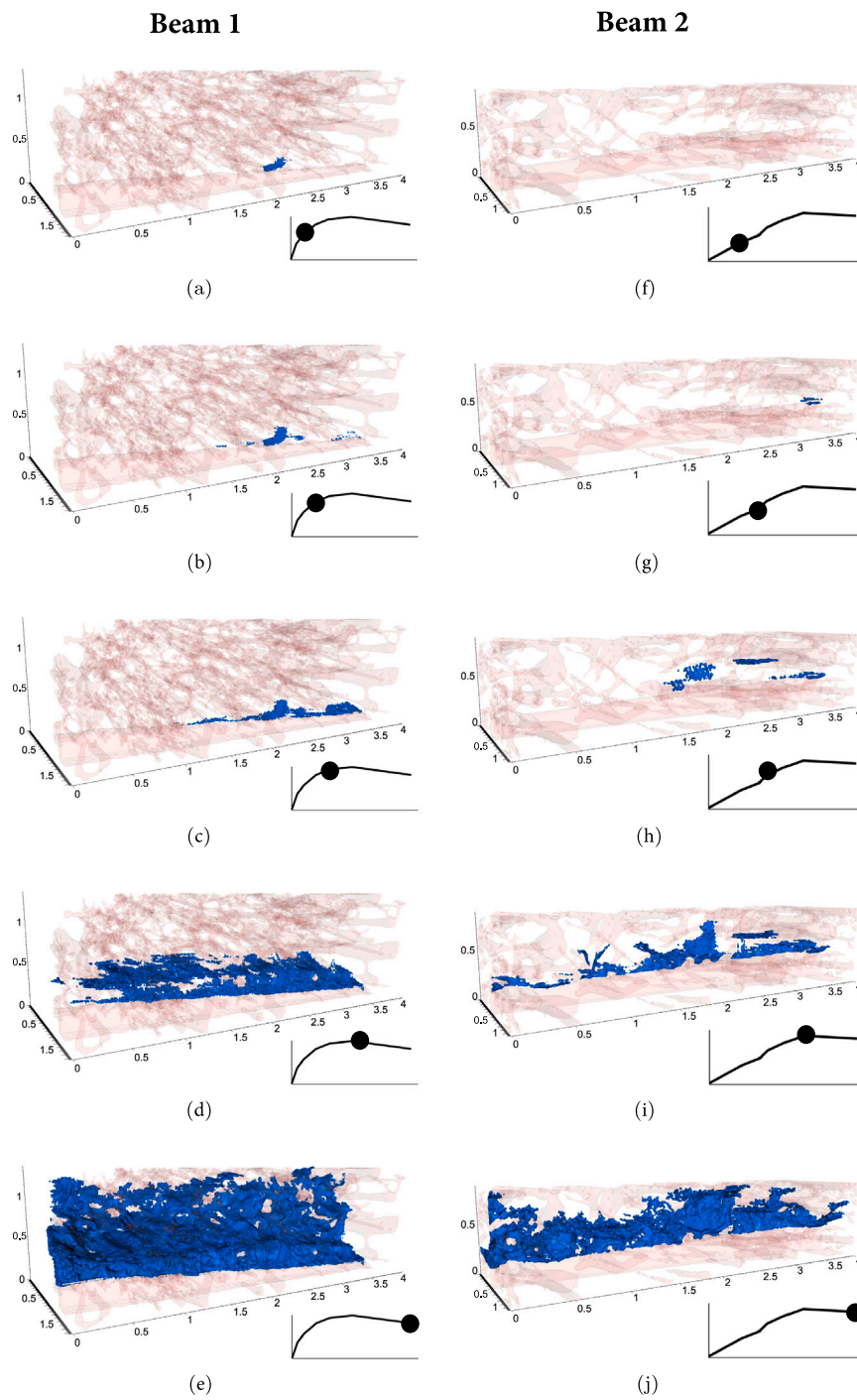


Fig. 3. 3D images of the development of the FPZ for (a–e) Beam 1, (f–j) Beam 2. Crack volume in blue, Haversian canals transparent red. All scale axes in mm. (For interpretation of the references to color in this figure legend, the reader is referred to the web version of this article.)

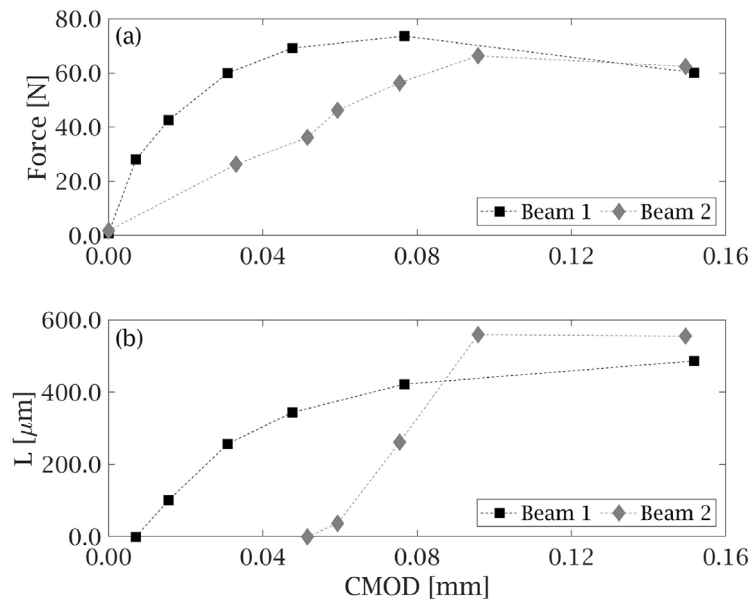


Fig. 4. (a) Force F vs. Crack Mouth Opening Displacement $CMOD$. (b) FPZ length L vs. $CMOD$. Lines as visual guide only.

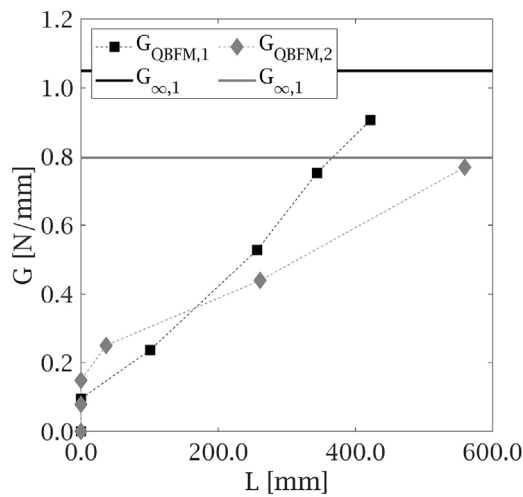


Fig. 5. Crack growth resistance curves in terms of G_{QBFM} vs. FPZ length L . Lines as visual guide only.

R -curves based on G_{QBFM} are in general agreement with values of J -integral following ASTM E1820, Supplementary Data. Values for initiation toughness in terms of J and G_{QBFM} are closely matching. During subsequent crack growth values of J exceed those for G_{QBFM} at an equivalent extension of the FPZ. We attribute such difference in part to the dissipation during the imaging holds, and to the potential for minor contributions to toughness from irreversible processes. R -curves in terms of J at first glance appear to indicate a lower fracture toughness of bone than reported in the literature (Koester et al., 2008; Granke et al., 2015; Dapaah and Willett, 2022). However, such data reported in the literature are based on crack extensions measured either optically at the free surface or from unloading compliance. Here we show that such measures can significantly underestimate the actual extension of the crack, Fig. 3. The formation of the FPZ starts at very low load values already and the local crack extension in the interior of the specimen happens significantly earlier than what can be detected at the specimen surface or can be noted in the unloading compliance.

QBFM is used to predict individual and combined effects of age, disease, and treatment on fracture risk. Fig. 8 allows one to assess potential treatment outcomes. Aging reduces Ct.Th (Thompson, 1980; Nguyen et al., 2018). Non-enzymatic collagen cross-linking and mineralization increase (Grynpas, 1993; Saito and Marumo, 2010), reducing deformation capacity. These effects would push a subject from baseline (center of Fig. 8B) towards a decreased load capacity in the bottom left of Fig. 8A and B. Anti-resorptive therapy either maintains (Chen et al., 2014; Niimi et al., 2015) or increases bone quantity (Seeman et al., 2010; Poole et al., 2015). Anti-resorptive treatments may decrease bone quality through increased mineral homogeneity, increasing brittleness (Grynpas, 1993), but not the degree of crack deflection (Acevedo et al., 2015). Depending on the actual treatment effect on bone quantity, anti-resorptive therapy may move a subject towards the bottom left corner of Fig. 8B or of Fig. 8C; hence with a stable or a slightly decreased load capacity. Bone ultrastructure composition also affects fracture toughness, Nyman et al. (2005). Improved toughness and post-yield behavior were observed in canine and murine bone treated by raloxifene or calcitonin without changes to bone quantity (Gallant et al., 2014; Surowiec et al., 2023). Improvements to bone health independent of quantity remain important avenues for new therapies for bone targeting extrinsic and intrinsic quality. Fig. 8 provides quantitative estimates of improvements in load-carrying capacity by improved intrinsic and extrinsic bone quality. High-resolution imaging techniques (Loundagain et al., 2021) and bone quality imaging (Jacobson et al., 2024) have advanced structural insights needed for FM analysis.

The present study provides initial steps in experiments and analysis in establishing the proposed method to potentially become fully established: specimens here are for method demonstration only. Following rules developed for engineering materials number of specimens required for statistical significance can be established to define a material-specific toughness. For bone, a notion of a subject-specific or bone type-specific fracture property might not exist as significant local variations appear significantly strong. While not addressed here, experimental measures should be obtained to understand differences between male/female subjects, changes with age, and among donors. These experiments were conducted in an ambient environment. Fracture experiments on sheep bone indicate experiments in air may overestimate crack growth resistance, but not crack initiation, relative to experiments in physiological solution (Shin et al., 2022).

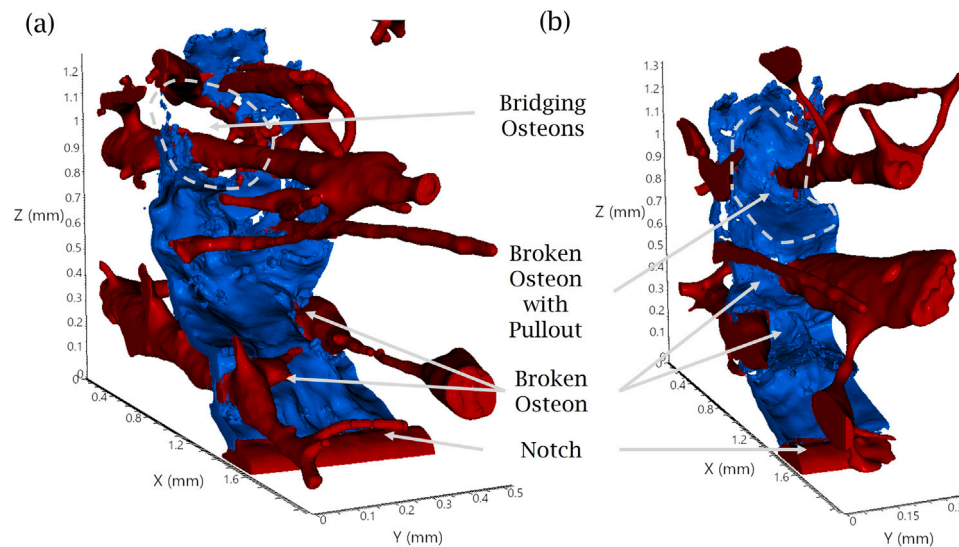


Fig. 6. Sections of Beam 1 segmented for the crack volume (blue) and Haversian Canals (red) after peak load when the FPZ is fully developed. Initial notch at the bottom of both images. (a&b): Broken osteons near the notch tip where the material is fully separated across the entire front of the initial crack. (a): Osteon bridging where a Haversian Canal crosses the fracture domain but remains surrounded by intact material. The cement line for this osteon is partially debonded. (b): Osteon pullout where a flat circular surface of the osteon faces against the crack volume and is surrounded by an area around the Haversian canal where the cement line has debonded and become part of the crack volume. (For interpretation of the references to color in this figure legend, the reader is referred to the web version of this article.)

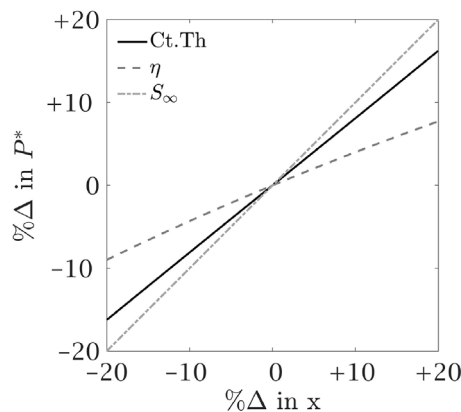


Fig. 7. Percent change in sustainable load, P^* , as a factor of percent change in cortical thickness Ct.Th, η , and S_∞ .

A more relevant question is that of validation. In the scope and length of the present paper, this step has not been included. In principle, data from a sub-sized FM specimen from one femur as described here should allow us to predict the load-carrying capacity of the other femur. Such a validation experiment encounters several issues, including but not limited to, asymmetry in shape and tissue characteristics, randomness in defects, and availability of donor tissue. One can argue that specimen availability issues can be overcome by the use of non-human bone, Kim et al. (2013). However, human bone is unique and the use of non-human bone will invariably lead to translational questions in return. Studies on human subjects are also needed, even if complex, in their donor-to-donor variability. One way to conduct such a validation would be to conduct a TPB fracture experiment on the whole bone first, then extract and test coupons from the undamaged sections, and use the QBFM data derived using these coupons to predict the whole bone failure. Alternatively, one can extract the test coupons from the proximal end of the femur diaphysis, and use a shortened diaphysis for the whole bone fracture experiment. We will conduct such experiments in future studies. While the present study did not include such original experiments, we validate our approach by the use of prior published data (Mather, 1967). Our method predicts a

maximum load in bending experiments of the femur well within the range of experimental data.

There are several readily possible extensions to the present version of the method. The QBFM approach developed here is isotropic but can be extended to account for anisotropy following Norman et al. (1995). Additional considerations on shape factors for the effects of the FPZ on G_{QBFM} would improve the accuracy of predictions (Di Luzio and Cusatis, 2018). The size extrapolation scheme can be extended by employing both FPZ length and FPZ width (Fakhimi and Tarokh, 2013; Galouei and Fakhimi, 2015; Tarokh et al., 2017) and potential modifications for bone microstructure. The present model is developed for femoral shaft fracture as the geometry is most amenable to closed-form analytical solutions. Investigations into other types of fracture, such as the important femur neck fracture, will require numerical solutions for the configuration functions which can be obtained following well-established procedures with the finite element method. The extrapolation approach developed in general FM terms (Fakhimi and Tarokh, 2013; Galouei and Fakhimi, 2015; Tarokh et al., 2017) should further be tested for the specific fracture processes in bone. Such work is currently underway. Future work will apply this approach to larger cohorts of donors but requires the use of high-throughput mechanical testing — for both fracture properties and elastic moduli.

5. Conclusions

This paper proposes to describe the fracture of advanced-age human cortical bone as a quasi-brittle material. Using the femoral cortical bone of a 92-year-old male, large-scale 3D imaging of transverse fractures reveals the fully developed fracture process zone (FPZ) to span multiple osteons. Cement lines are key to the formation of the FPZ and its advance. The large FPZ lengths cause a size effect in the fracture behavior. Given the anatomical constraints on specimen sizes, we posit that experiments on bending leading to transverse fracture will always lead to measurements of apparent, specimen size-specific fracture properties. In-situ loading experiments and QBFM analysis with a size-extrapolation approach are proposed to lead to the true tissue fracture properties. Such tissue fracture properties must be used to predict whole-bone strength. We postulate the existence of nonlinear mechanistic interaction effects between bone quantity and bone quality. There is a clear need to expand the number of measurements by including a

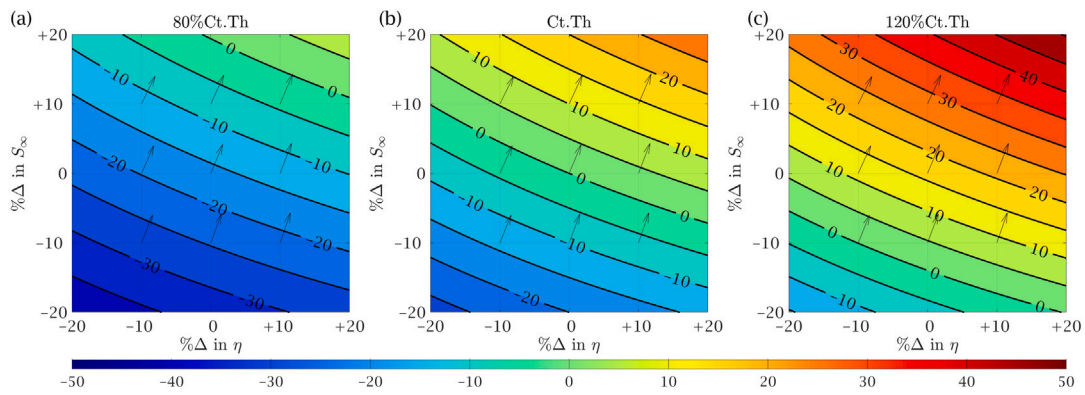


Fig. 8. Percent change in sustainable load, P^* , due to S_∞ and η at Ct.Th of (a) 80%, (b) 100%, and (c) 120% of the nominal cortical thickness.

larger number of specimens and donors, as well as to conduct direct validation studies of the QBFM methods in its application to human cortical bone.

CRedit authorship contribution statement

Glynn Gallaway: Writing – original draft, Visualization, Validation, Methodology, Investigation, Formal analysis, Data curation. **Rachel K. Surowiec:** Writing – review & editing, Visualization, Methodology, Investigation, Data curation. **Matthew R. Allen:** Writing – review & editing, Resources, Methodology, Funding acquisition, Conceptualization. **Joseph M. Wallace:** Writing – review & editing, Methodology, Funding acquisition, Conceptualization. **Laura J. Pyrak-Nolte:** Writing – review & editing, Methodology, Funding acquisition. **John A. Howarter:** Writing – review & editing, Methodology, Funding acquisition. **Thomas Siegmund:** Writing – original draft, Validation, Supervision, Project administration, Methodology, Investigation, Funding acquisition, Formal analysis, Data curation, Conceptualization.

Declaration of competing interest

We declare no conflict of interests.

Data availability

3D image stacks are available for the HRQCT scan of the femur bone and the individual load steps of the in-situ loading experiments, (Gallaway et al., 2024a). Data and analysis code are available in (Gallaway et al., 2024b).

Acknowledgments

This work is supported by the National Science Foundation award CMMI 1952993. G.G. is supported by the National Science Foundation award GRF DGE 1842166 and a Purdue University Doctoral Fellowship. We acknowledge the 3D X-ray microscope Facility in the Department of Physics, Purdue University, supported by the Purdue University 2017 Major Multi-User Equipment Program. The authors acknowledge the detailed comments on a possible validation method suggested by reviewers of this manuscript.

Appendix A. Supplementary data

Supplementary material related to this article can be found online at <https://doi.org/10.1016/j.jbiomech.2024.112359>.

References

- Acevedo, C., Bale, H., Gludovatz, B., Wat, A., Tang, S.Y., Wang, M., Busse, B., Zimmermann, E.A., Schaible, E., Allen, M.R., Burr, D.B., Ritchie, R.O., 2015. Alendronate treatment alters bone tissues at multiple structural levels in healthy canine cortical bone. *Bone* 81, 352–363.
- Aibar-Almazán, A., Voltes-Martínez, A., Castellote-Caballero, Y., Afanador-Restrepo, D.F., Carcelén-Fraile, M.d.C., López-Ruiz, E., 2022. Current status of the diagnosis and management of osteoporosis. *Int. J. Mol. Sci.* 23 (16).
- Ando, K., Kim, B.A., Iwasa, M., Ogura, N., 1992. Process zone size failure criterion and probabilistic fracture assessment curves for ceramics. *Fatigue Fract. Eng. Mater. Struct.* 15, 139–149.
- Barthelat, F., 2023. The fracture mechanics of biological materials. *CISM Int. Cent. Mech. Sci. Courses Lect.* 608, 255–282.
- Bartlow, C.M., Mann, K.A., Damron, T.A., Oest, M.E., 2018. Limited field radiation therapy results in decreased bone fracture toughness in a murine model. *PLoS One* 13, e0204928.
- Bažant, Z.P., 1984. Size effect in blunt fracture: Concrete, rock, metal. *J. Eng. Mech.* 110, 518–535.
- Bazant, Z.P., Kazemi, M.T., 1990. Determination of fracture energy, process zone length and brittleness number from size effect, with application to rock and concrete. *Int. J. Fract.* 44, 111–131.
- Bažant, Z.P., Kazemi, M.T., 1990. Size effect in fracture of ceramics and its use to determine fracture energy and effective process zone length. *J. Am. Ceram. Soc.* 73, 1841–1853.
- Bažant, Z.P., Li, Z., 1996. Zero-brittleness size-effect method for one-size fracture test of concrete. *J. Eng. Mech.* 122 (5), 458–468.
- Britz, H.M., Thomas, C.D.L., Clement, J.G., Cooper, D.M., 2009. The relation of femoral osteon geometry to age, sex, height and weight. *Bone* 45, 77–83.
- Carriero, A., Zimmermann, E.A., Shefelbine, S.J., Ritchie, R.O., 2014. A methodology for the investigation of toughness and crack propagation in mouse bone. *J. Mech. Behav. Biomed. Mater.* 39, 38–47.
- Chen, F., Wang, Z., Bhattacharyya, T., 2014. Absence of femoral cortical thickening in long-term bisphosphonate users: Implications for atypical femur fractures. *Bone* 62, 64–66.
- Dapaah, D., Martel, D.R., Iranmanesh, F., Seelemann, C., Laing, A.C., Willett, T., 2023. Fracture toughness: Bridging the gap between hip fracture and fracture risk assessment. *Curr. Osteoporos. Rep.* 21, 253–265.
- Dapaah, D., Martel, D.R., Laing, A.C., Willett, T.L., 2022. The impact of fall-related loading rate on the formation of micro-damage in human cortical bone fracture. *J. Biomech.* 142, 111254.
- Dapaah, D., Willett, T., 2022. A critical evaluation of cortical bone fracture toughness testing methods. *J. Mech. Behav. Biomed. Mater.* 134, 105419.
- Demirtas, A., Taylor, E.A., Gludovatz, B., Ritchie, R.O., Donnelly, E., Ural, A., 2023. An integrated experimental-computational framework to assess the influence of microstructure and material properties on fracture toughness in clinical specimens of human femoral cortical bone. *J. Mech. Behav. Biomed. Mater.* 145, 106034.
- Di Luzio, G., Cusatis, G., 2018. Cohesive crack analysis of size effect for samples with blunt notches and generalized size effect curve for quasi-brittle materials. *Eng. Fract. Mech.* 204, 15–28.
- Fakhimi, A., Tarokh, A., 2013. Process zone and size effect in fracture testing of rock. *Int. J. Rock Mech. Min. Sci.* 60, 95–102.
- Gallant, M.A., Brown, D.M., Hammond, M., Wallace, J.M., Du, J., Deymier-Black, A.C., Almer, J.D., Stock, S.R., Allen, M.R., Burr, D.B., 2014. Bone cell-independent benefits of raloxifene on the skeleton: A novel mechanism for improving bone material properties. *Bone* 61, 191–200.

- Galloway, G., Allen, M.R., Surowiec, R.K., Siegmund, T., 2024a. 3D image data from in-situ X-ray imaging of transverse crack growth experiments in human cortical bone. Purdue University Research Repository, <http://dx.doi.org/10.4231/94PZ-AB06>.
- Galloway, G., Pyrak-Nolte, L.J., Siegmund, T., 2024b. Load data and code for analysis of in-situ X-ray transverse crack growth experiments in specimens of a human cortical bone. Purdue University Research Repository, <http://dx.doi.org/10.4231/RWPA-PG56>.
- Galouei, M., Fakhimi, A., 2015. Size effect, material ductility and shape of fracture process zone in quasi-brittle materials. *Comput. Geotech.* 65, 126–135.
- Ghoulis, S., Ayatollahi, M.R., Bahrami, B., Jamali, J., 2022. In-situ optical approach to predict mixed mode fracture in a polymeric biomaterial. *Theor. Appl. Fract. Mech.* 118, 103211.
- Giannoudis, P., Tzioupi, C., Almalli, T., Buckley, R., 2007. Fracture healing in osteoporotic fractures: Is it really different?: A basic science perspective. *Injury* 38, S90–S99.
- Granke, M., Makowski, A.J., Uppuganti, S., Does, M.D., Nyman, J.S., 2015. Identifying novel clinical surrogates to assess human bone fracture toughness. *J. Bone Miner. Res.* 30 (7), 1290–1300.
- Grynblas, M., 1993. Age and disease-related changes in the mineral of bone. *Calcif. Tissue Int.* 53, S57–S64.
- Guinea, G.V., Planas, J., Elices, M., 1998. Stress intensity factor, compliance and CMOD for a general three-point-bend beam. *Int. J. Fract.* 89, 103–116.
- Gustafsson, A., Wallin, M., Khayyeri, H., Isaksson, H., 2019. Crack propagation in cortical bone is affected by the characteristics of the cement line: a parameter study using an XFEM interface damage model. *Biomech. Model. Mechanobiol.* 18, 1247–1261.
- Hernandez, C., Keaveny, T., 2006. A biomechanical perspective on bone quality. *Bone* 39 (6), 1173–1181.
- Hernandez, C.J., van der Meulen, M.C., 2017. Understanding bone strength is not enough. *J. Bone Miner. Res.* 32 (6), 1157–1162.
- Idkaidek, A., Jasiuk, I., 2017. Cortical bone fracture analysis using XFEM – case study. *Int. J. Numer. Methods Biomed. Eng.* 33, e2809.
- Jacobson, A.M., Zhao, X., Sommer, S., Sadik, F., Warden, S.J., Newman, C., Siegmund, T., Allen, M.R., Surowiec, R.K., 2024. A comprehensive set of ultrashort echo time magnetic resonance imaging biomarkers to assess cortical bone health: A feasibility study at clinical field strength. *Bone* 117031.
- Kanis, J.A., Johnell, O., Oden, A., Jonsson, B., Laet, C.D., Dawson, A., 2000. Risk of hip fracture according to the world health organization criteria for osteopenia and osteoporosis. *Bone* 27, 585–590.
- Karali, A., Kao, A.P., Zekonyte, J., Blunn, G., Tozzi, G., 2021. Micromechanical evaluation of cortical bone using in situ XCT indentation and digital volume correlation. *J. Mech. Behav. Biomed. Mater.* 115, 104298.
- Kasiri, S., Taylor, D., 2008. A critical distance study of stress concentrations in bone. *J. Biomech.* 41, 603–609.
- Kim, K.T., Bažant, Z.P., Yu, Q., 2013. Non-uniqueness of cohesive-crack stress-separation law of human and bovine bones and remedy by size effect tests. *Int. J. Fract.* 181, 67–81.
- Koester, K.J., Ager, J.W., Ritchie, R.O., 2008. The true toughness of human cortical bone measured with realistically short cracks. *Nat. Mater.* 7, 672–677, 2008 7:8.
- Launey, M.E., Buehler, M.J., Ritchie, R.O., 2010. On the mechanistic origins of toughness in bone. *Annu. Rev. Mater. Res.* 40, 25–53.
- Leucht, S., Helfer, B., Gartlehner, G., Davis, J.M., 2015. How effective are common medications: A perspective based on meta-analyses of major drugs. *BMC Med.* 13, 1–5.
- Lloyd, A.A., Gludovatz, B., Riedel, C., Luengo, E.A., Saiyed, R., Marty, E., Lorch, D.G., Lane, J.M., Ritchie, R.O., Busse, B., et al., 2017. Atypical fracture with long-term bisphosphonate therapy is associated with altered cortical composition and reduced fracture resistance. *Proc. Natl. Acad. Sci.* 114 (33), 8722–8727.
- Loundagain, L.L., Bredbenner, T.L., Jepsen, K.J., Edwards, W.B., 2021. Bringing mechanical context to image-based measurements of bone integrity. *Curr. Osteoporos. Rep.* 19, 542–552.
- Lowe, T., Avcu, E., Bousser, E., Sellers, W., Withers, P.J., 2018. 3D imaging of indentation damage in bone. *Materials* 11, 2533, 2018, Vol. 11, Page 2533.
- Lu, Y., Genant, H.K., Shepherd, J., Zhao, S., Mathur, A., Fuerst, T.P., Cummings, S.R., 2001. Classification of osteoporosis based on bone mineral densities. *J. Bone Miner. Res.* 16, 901–910.
- Mather, B.S., 1967. Correlations between strength and other properties of long bones. *J. Trauma Acute Care Surg.* 7 (5), 633–638.
- Mirzaali, M.J., Schwiedrzik, J.J., Thaiwichai, S., Best, J.P., Michler, J., Zysset, P.K., Wolfram, U., 2016. Mechanical properties of cortical bone and their relationships with age, gender, composition and microindentation properties in the elderly. *Bone* 93, 196–211.
- Moazzami, M., Ayatollahi, M.R., Akhavan-Safar, A., 2020. Assessment of the fracture process zone in rocks using digital image correlation technique: The role of mode-mixity, size, geometry and material. *Int. J. Damage Mech.* 29, 646–666.
- Morgan, S.P., Johnson, C.A., Einstein, H.H., 2013. Cracking processes in barre granite: Fracture process zones and crack coalescence. *Int. J. Fract.* 180, 177–204.
- Nalla, R.K., Kruzic, J.J., Kinney, J.H., Balooch, M., Ager, J.W., Ritchie, R.O., 2006. Role of microstructure in the aging-related deterioration of the toughness of human cortical bone. *Mater. Sci. Eng. C* 26, 1251–1260.
- Nalla, R.K., Kruzic, J.J., Kinney, J.H., Ritchie, R.O., 2004a. Effect of aging on the toughness of human cortical bone: evaluation by R-curves. *Bone* 35, 1240–1246.
- Nalla, R.K., Kruzic, J.J., Kinney, J.H., Ritchie, R.O., 2005. Mechanistic aspects of fracture and R-curve behavior in human cortical bone. *Biomaterials* 26, 217–231.
- Nalla, R.K., Kruzic, J.J., Ritchie, R.O., 2004b. On the origin of the toughness of mineralized tissue: microcracking or crack bridging? *Bone* 34, 790–798.
- Nguyen, B.N., Hoshino, H., Togawa, D., Matsuyama, Y., 2018. Cortical thickness index of the proximal femur: A radiographic parameter for preliminary assessment of bone mineral density and osteoporosis status in the age 50 years and over population. *Clin. Orthop. Surg.* 10, 149–156.
- Niimi, R., Kono, T., Nishihara, A., Hasegawa, M., Matsumine, A., Kono, T., Sudo, A., 2015. Cortical thickness of the femur and long-term bisphosphonate use. *J. Bone Miner. Res.* 30, 225–231.
- Norman, T.L., Vashishth, D., Burr, D., 1995. Fracture toughness of human bone under tension. *J. Biomech.* 28 (3), 309–320.
- Nyman, J.S., Reyes, M., Wang, X., 2005. Effect of ultrastructural changes on the toughness of bone. *Micron* 36, 566–582.
- Peña Fernández, M., Kao, A.P., Witte, F., Arora, H., Tozzi, G., 2020. Low-cycle full-field residual strains in cortical bone and their influence on tissue fracture evaluated via in situ stepwise and continuous X-ray computed tomography. *J. Biomech.* 113, 110105.
- Poole, K.E., Treece, G.M., Gee, A.H., Brown, J.P., McClung, M.R., Wang, A., Libanati, C., 2015. Denosumab rapidly increases cortical bone in key locations of the femur: A 3D bone mapping study in women with osteoporosis. *J. Bone Miner. Res.* 30, 46–54.
- Ritchie, R., Koester, K., Ionova, S., Yao, W., Lane, N., Ager, J., 2008. Measurement of the toughness of bone: A tutorial with special reference to small animal studies. *Bone* 43 (5), 798–812.
- Saito, M., Marumo, K., 2010. Collagen cross-links as a determinant of bone quality: A possible explanation for bone fragility in aging, osteoporosis, and diabetes mellitus. *Osteoporos. Int.* 21, 195–214.
- Schmidt, F.N., Hahn, M., Stockhausen, K.E., Rolvien, T., Schmidt, C., Knopp, T., Schulze, C., Püschel, K., Amling, M., Busse, B., 2022. Influence of X-rays and gamma-rays on the mechanical performance of human bone factoring out in-traindividual bone structure and composition indices. *Mater. Today Biol.* 13, 100169.
- Schuit, S., van der Klift, M., Weel, A., de Laet, C., Burger, H., Seeman, E., Hofman, A., Uitterlinden, A., van Leeuwen, J., Pols, H., 2004. Fracture incidence and association with bone mineral density in elderly men and women: the Rotterdam study. *Bone* 34 (1), 195–202.
- Seeman, E., Delmas, P.D., Hanley, D.A., Sellmeyer, D., Cheung, A.M., Shane, E., Kearns, A., Thomas, T., Boyd, S.K., Boutroy, S., Bogado, C., Majumdar, S., Fan, M., Libanati, C., Zanchetta, J., 2010. Microarchitectural deterioration of cortical and trabecular bone: Differing effects of denosumab and alendronate. *J. Bone Miner. Res.* 25, 1886–1894.
- Shin, M., Zhang, M., vom Scheidt, A., Pelletier, M.H., Walsh, W.R., Martens, P.J., Kruzic, J.J., Busse, B., Gludovatz, B., 2022. Impact of test environment on the fracture resistance of cortical bone. *J. Mech. Behav. Biomed. Mater.* 129, 105155.
- Surowiec, R.K., Saldívar, R., Rai, R.K., Metzger, C.E., Jacobson, A.M., Allen, M.R., Wallace, J.M., 2023. Ex vivo exposure to calcitonin or raloxifene improves mechanical properties of diseased bone through non-cell mediated mechanisms. *Bone* 173, 116805.
- Tarokh, A., Makhnenko, R.Y., Fakhimi, A., Labuz, J.F., 2017. Scaling of the fracture process zone in rock. *Int. J. Fract.* 204, 191–204.
- Teng, G.G., Curtis, J.R., Saag, K.G., 2008. Mortality and osteoporotic fractures: is the link causal, and is it modifiable? *Clin. Exp. Rheumatol.* 26, S125–S137.
- Thompson, D.D., 1980. Age changes in bone mineralization, cortical thickness, and Haversian canal area. *Calcif. Tissue Int.* 31, 5–11.
- Tsouvalis, N.G., Anyfantis, K.N., 2012. Determination of the fracture process zone under mode I fracture in glass fiber composites. *J. Compos. Mater.* 46, 27–41.
- Vashishth, D., Behiri, J.C., Bonfield, W., 1997. Crack growth resistance in cortical bone: Concept of microcrack toughening. *J. Biomech.* 30, 763–769.
- Wu, Z.M., Rong, H., Zheng, J.J., Xu, F., Dong, W., 2011. An experimental investigation on the FPZ properties in concrete using digital image correlation technique. *Eng. Fract. Mech.* 78, 2978–2990.
- Yang, Q.D., Cox, B.N., Nalla, R.K., Ritchie, R.O., 2006. Fracture length scales in human cortical bone: The necessity of nonlinear fracture models. *Biomaterials* 27, 2095–2113.
- Yeni, Y.N., Brown, C.U., Wang, Z., Norman, T.L., 1997. The influence of bone morphology on fracture toughness of the human femur and tibia. *Bone* 21, 453–459.

Zimmermann, E.A., Launey, M.E., Ritchie, R.O., 2010. The significance of crack-resistance curves to the mixed-mode fracture toughness of human cortical bone. *Biomaterials* 31, 5297–5305.

Zimmermann, E.A., Schaible, E., Bale, H., Barth, H.D., Tang, S.Y., Reichert, P., Busse, B., Alliston, T., Ager, J.W., Ritchie, R.O., 2011. Age-related changes in the plasticity and toughness of human cortical bone at multiple length scales. *Proc. Natl. Acad. Sci. USA* 108, 14416.

Ziopoulos, P., Currey, J.D., 1998. Changes in the stiffness, strength, and toughness of human cortical bone with age. *Bone* 22, 57–66.